PHYSICAL REVIEW B **78**, 161402(R) (2008)

# Describing bond-breaking processes by reactive potentials: Importance of an environment-dependent interaction range

Lars Pastewka,[1] Pablo Pou,[2,3] Rubén Pérez,[3] Peter Gumbsch,[1,2] and Michael Moseler[1,4,*]
[1]*Fraunhofer-Institut für Werkstoffmechanik (IWM), Wöhlerstraße 11, D-79108 Freiburg, Germany*
[2]*IZBS, Universität Karlsruhe, Kaiserstraße 12, D-76131 Karlsruhe, Germany*
[3]*Departamento de Física Teórica de la Materia Condensada, UAM, E-28049 Madrid, Spain*
[4]*Freiburger Materialforschungszentrum, Stefan-Meier-Straße 21, D-79104 Freiburg, Germany*
(Received 28 July 2008; published 7 October 2008)

First nearest-neighbor models are routinely used for atomistic modeling of covalent materials. Neighbors are usually determined by looking for atoms within a fixed interaction range. While these models provide a faithful description of material properties near equilibrium, the limited interaction range introduces problems in heterogeneous environments and when bond-breaking processes are of concern. We demonstrate in this Rapid Communication that the reliability of reactive bond-order potentials is substantially improved by using an environment-dependent first nearest-neighbor definition.

DOI: 10.1103/PhysRevB.78.161402 PACS number(s): 68.35.Af, 34.20.Cf, 62.20.mj, 62.20.mt

Many physical processes in condensed matter are studied by molecular dynamics employing empirical interatomic potentials.[1] Millions of atoms and micron-scale systems are now accessible by order-$N$ scaling techniques.[2] This is closely related to a rigorous reduction of the interaction range $r_c$ in the employed empirical potentials. While metallic potentials usually involve at least third nearest neighbors (NN),[1] state-of-the-art covalent potentials consider first NN bonds only.[3–5] Unfortunately, there is a serious problem related to the drastic reduction of $r_c$. In general, one can state that the faster a bond energy vanishes as a function of distance, the larger the forces required for bond breaking. This leads to a serious overestimation of critical loads and shear stresses in fracture mechanics and tribology, which existing potentials fail to describe properly.[6,7]

In this Rapid Communication, this failure is demonstrated and cured for the Brenner bond-order potential (BBOP).[3] This prominent hydrocarbon potential has been designed to give reasonable estimates for the energetics and structures of solid phases and molecules and it has been successfully used in numerous studies.[8] Figure 1 illustrates three problematic cases. A crack tip in diamond shows artificial blunting [Fig. 1(a)] instead of an expected brittle fracture.[9] Experimentally, carbon nanotubes break brittle at low temperatures,[10] while BBOP predicts a ductile necking [Fig. 1(b)]. Furthermore, a shear-induced diamond-to-graphite transition[11,12] is not captured correctly [Fig. 1(c)]. The BBOP critical shear stresses (72 GPa and 75 GPa for a positive and a negative shearing direction, respectively[13]) underestimate corresponding reference values (175 GPa and 95 GPa) from density-functional theory (DFT) calculations.[11] Even worse, the ordering of these values is reversed and the final structure is wrong for one shear direction.

Likewise, structural problems arising in the description of amorphous carbon (a-C) materials[14] (essentially a misestimation of the $sp^2/sp^3$ phase equilibrium) can be traced back to a too small $r_c$. Naively extending $r_c$ to include further neighbor shells changes the potentials' properties (e.g., leading to too weak elastic behavior and a tendency to close-packed structures), since bond integrals for more distant neighbors can generally not be determined by extrapolation of first NN interaction energies.[15]

In this work, we retain the idea of considering first NN interactions only while dynamically adjusting $r_c$ depending on the local atomic environment of a bond. This can be achieved by determining NNs from a criterion other than distance. We show that empirical screening functions as introduced by Baskes[16] can be combined with BBOP to a computationally efficient scheme that avoids the aforementioned deficiencies. This procedure can be considered an empirical incarnation of analytic bond-order formulations which directly mimic environment dependence of bond integrals using screening functions.[17] The screening approach has to be distinguished from coordination-dependent short-range cutoff procedures[18] that only improve equilibrium properties without fixing the bond-breaking problem.

The original BBOP total energy[3] which we use in this work[19] is given by a sum over repulsive ($V_r$) and attractive pair potentials ($V_a$)

$$E = \sum_{i<j} [V_r(r_{ij}) + b_{ij} V_a(r_{ij})] f_c(r_{ij}). \tag{1}$$

Here $r_{ij}$ denotes the distance between atom $i$ and $j$, $b_{ij}$ the bond order, and $f_c$ a cutoff function[3] which smoothly zeroes the interaction beyond a critical distance. In the following, we propose a modified cutoff scheme [Fig. 2(a)] that uses this simple formulation only for very small $r_{ij}$. For larger $r_{ij}$, the interaction might be reduced by a third atom $k$. We consider a bond between atoms $i$ and $j$ to be entirely screened by atom $k$ if the coefficient

$$C_{ijk} = \frac{2(X_{ik} + X_{jk}) - (X_{ik} - X_{jk})^2 - 1}{1 - (X_{ik} - X_{jk})^2} \tag{2}$$

falls below a critical value $C_{\min}$, while an unscreened bond corresponds to $C_{ijk} > C_{\max}$. Here, $X_{ik} = (r_{ik}/r_{ij})^2$ and a geometric explanation for this coefficient is given in Fig. 2(b) or Ref. 16. The total screening function $S_{ij}$ is then given by $S_{ij} = 0$ if the bond $ij$ is entirely screened and otherwise by

 ©2008 The American Physical Society

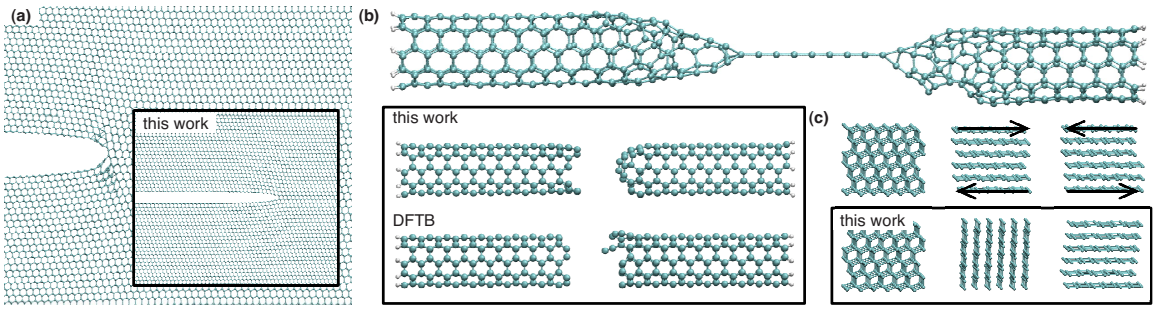


FIG. 1. (Color online) The failure of the original Brenner potential. (a) A crack on a diamond (111) plane with a [110] crack front shows crack tip blunting and does not propagate at 10% strain in contrast to common experimental wisdom. (b) Quasistatically pulling a 5,5 carbon nanotube leads to ductile behavior whereas quantum calculations and low-temperature experiments predict brittle fracture. (c) Diamond transforms to graphite under shear loading. In addition to underestimating the necessary shear stress, the Brenner potential shows the wrong transition behavior in one of the loading directions. DFT calculations predict a different rotation of the graphene planes after the transition for the "positive" (left) and "negative" (right) shear direction. Insets: Results obtained using the modifications presented in this paper.

$$S_{ij} = \prod_{k,C_{ijk}<C_{\max}} \exp\left[-\left(\frac{C_{\max}-C_{ijk}}{C_{ijk}-C_{\min}}\right)^2\right]. \tag{3}$$

Finally, a modified cutoff function is defined by

$$f_c(r_{ij}) = f_c^{12}(r_{ij}) + [1 - f_c^{12}(r_{ij})] f_c^{34}(r_{ij}) S_{ij}, \tag{4}$$

where $f_c^{12}(r)$ is the original and $f_c^{34}(r)$ an additional cutoff function. The former switches the interaction off between radii $r_1$ and $r_2$ and the latter between $r_3$ and $r_4$ [Fig. 2(a)]. These functions are identical to those used in the original formulation of the potential.[3] Equations (2)–(4) can be regarded as an empirical recipe. Reference 17 proposed a physically motivated scheme for angular screening in the same context, which does not have the simplicity and numerical efficiency of the approach presented here. Considering the empirical nature of the original BBOP we felt that Eqs. (2)–(4) are more adequate.

Table I documents our choice of $r_1$, $r_2$, $r_3$, $r_4$, $C_{\min}$, and $C_{\max}$. These parameters were determined as follows. We considered the work of separation $E_{111}(z)$ and $E_{110}(z)$ of two unrelaxed diamond (111) and (110) surfaces, respectively. Here, $z$ is the separation of the surfaces. The cutoff parameters were identified by requiring smoothness of these functions such that the square of their second derivatives were minimized while restricting the maximum cutoff to 4.0 Å. This fit did not involve additional *ab initio* data but gave reasonable agreement with *ab initio* calculations [inset in Fig. 4(b)]. Spurious wells in the cohesive force functions, $-\partial E_{111}(z)/\partial z$ and $-\partial E_{110}(z)/\partial z$, were removed by choosing individual $r_3$ and $r_4$ values for the pair potentials $V_a$ and $V_r$ ($r_{3ar}$, $r_{4ar}$), the $b_{ij}$ formula, and the dihedral energy ($r_{3bd}$, $r_{4bd}$), as well as for the neighbor and conjugation cutoffs occurring in $b_{ij}$ ($r_{3nc}$, $r_{4nc}$).

The parameters $C_{\min}$ and $C_{\max}$ were restricted to the range between triangular ($C_{\max} \leq 3$) and square structures ($C_{\min} \geq 1$) and were optimized to reproduce hybridization curves for amorphous carbon. Both values were sampled in steps of 0.1, and we found that in the vicinity of $C_{\min}=1.0$ and $C_{\max}=2.0$ the results were closest to those obtained by other methods (see Fig. 3) within the error bars from ten independent runs. Amorphous carbon (a-C) samples with 512 atoms were quenched from the melt similar to previous studies that employed DFT (Refs. 20 and 21) or density-functional-based tight binding (DFTB).[22] Temperature control was achieved by velocity rescaling. After 0.5 ps equilibration at 5000 K the sample was cooled down exponentially to 300 K in 0.5 ps, followed again by 0.5 ps of equilibration. The resulting structure was analyzed with respect to $sp^3$ content, as well as pair distribution and ring statistics.[23]

Figure 3 compares the results of our simulation with

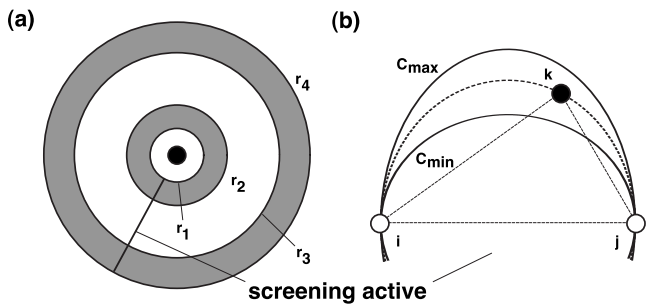


FIG. 2. Cutoff formulation for the bond $ij$. (a) Four cutoff radii are used. The interaction is always computed if $r_{ij}<r_1$. For $r_1<r_{ij}<r_4$ screening is considered. The inner gray region switches between these two cases and the outer gray region smoothly zeroes the potential. (b) Screening of the bond $ij$: Ellipses (dashed-line) are constructed through all third atoms $k$ with $i$-$j$ being the first half axis. The coefficient $C_{ijk}$ is then given by the square of the fraction of the second half axis to the first half axis. For further details see text.

TABLE I. Radii and critical $C_{\min/\max}$ used for the hydrocarbon potential. Note that in this parametrization two graphite planes interact and the interplane distance has a local minimum at 3.34 Å. The cohesive energy of graphite is −7.41 eV.

| $r_1$[Å] | $r_2$[Å] | | $C_{\min}$ | $C_{\max}$ |
|---|---|---|---|---|
| 1.95 | 2.25 | | 1.0 | 2.0 |
| $r_{3ar}$[Å] | $r_{4ar}$[Å] | $r_{3bd}$[Å] | $r_{4bd}$[Å] | $r_{3nc}$[Å] | $r_{4nc}$[Å] |
| 2.179347 | 2.819732 | 1.866344 | 2.758372 | 1.217335 | 4.0 |

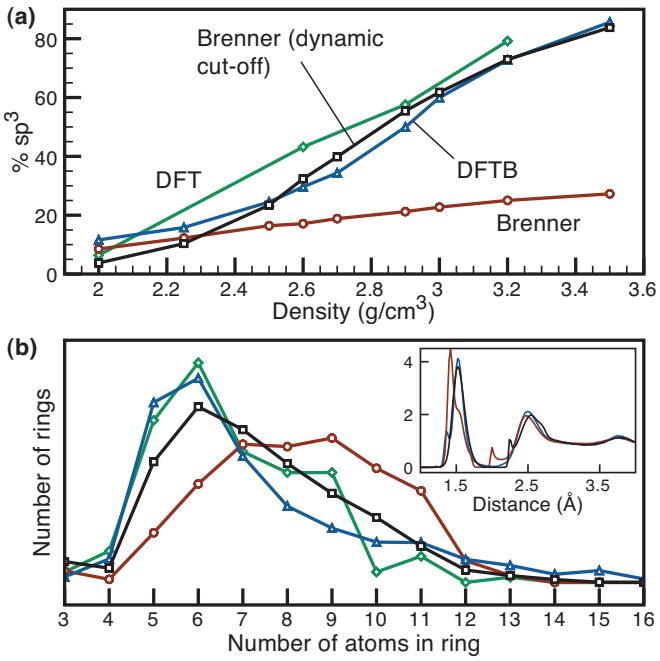


FIG. 3. (Color) Properties of quenched a-C. (a) Hybridization (fraction of $sp^3$ sites) as a function of density for a-C. (b) Ring statistics of the a-C samples at a density of 2.9 $g/cm^3$. Inset: Pair distribution for the same samples. The data has been averaged over ten consecutive runs. 512 atom samples are used in the Brenner and DFTB calculations while the DFT data was computed using 64 atom samples (Ref. 21). The hybridization was determined by counting neighbors within a cutoff of 1.85 Å.

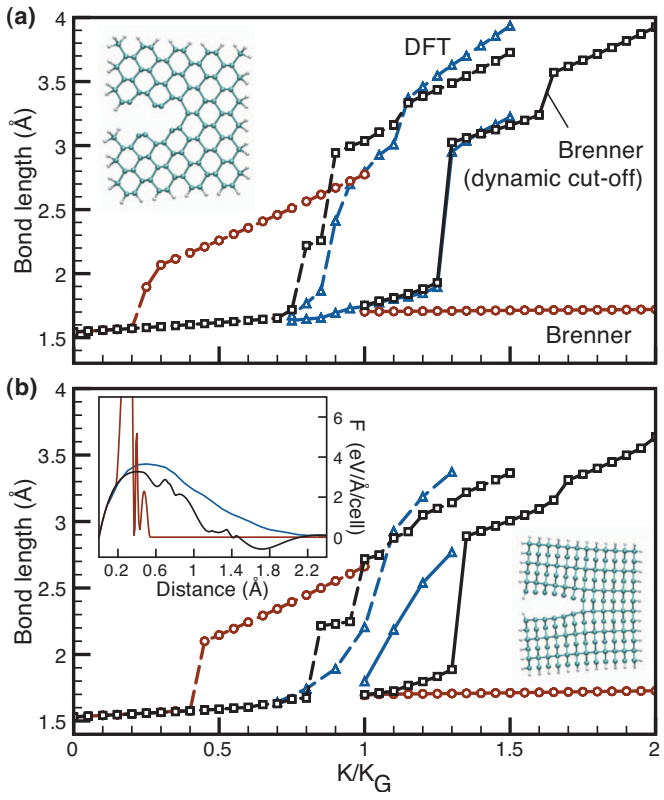


FIG. 4. (Color) Crack propagation on the diamond (110) plane. Solid lines give the bond length of the bond behind the crack tip for an increasing stress intensity factor (loading). For a decreasing stress intensity factor (unloading) the bond length of the bond in front of the crack tip is displayed. These are the dashed lines. The stress intensities are increased in steps of $0.05K_G$. For more information on the DFT calculations and the specific crack configuration used see Refs. 25 and 26. (a) $[1\bar{1}0]$ crack front (b) [001] crack front. Inset: Cohesive force function $\partial E_{110}(z)/\partial z$ of the unrelaxed diamond (110) surface as a function of surface separation $z$.

DFT,[20,21] DFTB (Ref. 22) calculations, and the unscreened BBOP. An almost perfect match with the hybridization [Fig. 3(a)] of the quantum reference is found over a range of densities when introducing the screening approach with the appropriate $C_{\max}$ and $C_{\min}$.[24] In ring statistics, the majority of rings are now shifted from around nine atoms to six atoms, substantially improving the agreement with quantum calculations [Fig. 3(b)]. The same holds for the radial distribution function [inset of Fig. 3(b)].

In order to evaluate the performance of our modified Brenner potential, we consider two examples: fracture on a diamond (110) crack plane (Fig. 4) and a shear-induced diamond to graphite transition [Fig. 1(c)]. Fracture in diamond is investigated by considering a small atomistic region around a crack tip that is either aligned along the $[1\bar{1}0]$ or the [001] direction [see Fig. 4(a) and Fig. 4(b), respectively] and employing mode $I$ near field solution of continuum fracture theory to the boundaries.[25,26] The stress intensity factor $K$ is stepwise increased and after each step the system is relaxed to the ground state using the fast inertial relaxation engine.[27] Figure 4 displays the bond length at the crack tip as a function of $K/K_G$. Results from the original unscreened[24] and our screened BBOP are compared with reference DFT calculations.[28]

Without screening functions, the bond never breaks up to $K=2K_G$ and rejoins at a much too low $K<0.6K_G$ when starting from an initially open configuration. Including screening functions, the bond breaks properly. This is because the maximum of the cohesive force function, as shown in the inset in Fig. 4(b), approximately matches the results from the DFT calculations. Its shape does however show spurious oscillations. These are attributable to the treatment of the $\pi$ electrons within the Brenner potential. The interpolation prescription for the $F$ tables in Ref. 3 leads to unphysical energy barriers when bonds are collectively broken.

For the $[1\bar{1}0]$ crack front the ratio of the stress intensities at which bonds break or rejoin $\Delta K=K^+-K^-$ to the critical stress intensities $\Delta K/K_G$ which describes lattice trapping are in quantitative agreement with the DFT. On the other hand, our potential does not reproduce the smooth opening of the bond which is seen in DFT calculations of the easy [001] crack front. The smooth opening of bonds in the latter case is most likely an effect caused by the details of the electron density at the crack tip. Apart from this minor discrepancy, we can conclude that screening improves the fracture mechanics of BBOP considerably leading to the correct brittle behavior in diamond [Fig. 1(a)] and in nanotubes [Fig. 1(b)].

Finally, we apply the screened BBOP to the transition from diamond to graphite under shear following the route in

Ref. 11. For both, positive and negative shear we find a transformation into the same graphitic structure as the DFT calculations[11] [see Fig. 1(c)]. Critical stresses are 285 GPa and 150 GPa for the positive and negative shear direction, respectively. While this is an overestimation of the 175 and 95 GPa obtained from DFT calculations,[11] the modifications to the Brenner potential do lead to the proper structures and a proper ordering of the shear stresses.

We would like to point out that initial tests on the silicon-carbide potential of Tersoff[5] show similarly encouraging results. This fosters the expectation that the introduction of an environment-dependent cutoff into simple bond-order potentials will pave the way to reliable large-scale simulations of fracture and friction in covalent materials.

The authors would like to thank Matous Mrovec for fruitful discussion. Funding was provided by the Fraunhofer project "CarNAk" and the BMBF project "OTRISKO."

*Author to whom correspondence should be addressed; michael.moseler@iwm.fraunhofer.de

[1] M. Finnis, *Interatomic Forces in Condensed Matter* (Oxford University Press, Oxford, 2004).

[2] M. P. Allen and D. J. Tildesley, *Computer Simulation of Liquids* (Clarendon, Oxford, 1989).

[3] D. W. Brenner, O. A. Shenderova, J. A. Harrison, S. J. Stuart, B. Ni, and S. B. Sinnott, J. Phys.: Condens. Matter **14**, 783 (2002).

[4] D. G. Pettifor and I. I. Oleinik, Phys. Rev. B **59**, 8487 (1999).

[5] J. Tersoff, Phys. Rev. B **39**, 5566 (1989).

[6] P. Gumbsch, *Materials Science for the 21st Century* (The Society of Materials Science, JSMS, Japan, 2001), Vol. A, pp. 50–58.

[7] M. Marder, Comput. Sci. Eng. **1**, 48 (1999).

[8] J. A. Harrison, G. Gao, J. D. Schall, M. T. Knippenberg, and P. T. Mikulski, Philos. Trans. R. Soc. London, Ser. A **366**, 1469 (2008).

[9] J. E. Field, *The Properties of Natural and Synthetic Diamond* (Academic, London, 1992).

[10] M. Marques, H. Troiani, M. Miki-Yoshida, M. Jose-Yacaman, and A. Rubio, Nano Lett. **4**, 811 (2004).

[11] H. Chacham and L. Kleinman, Phys. Rev. Lett. **85**, 4904 (2000).

[12] Y. G. Gogotsi, A. Kailer, and K. G. Nickel, Nature (London) **401**, 663 (1999).

[13] Following Ref. 11, the crystal is sheared by applying a strain in the $[2\bar{1}\bar{1}]$ direction and relaxing in the [111] direction. The "positive" and "negative" shear direction is defined in Fig. 1.

[14] H. U. Jäger and K. Albe, J. Appl. Phys. **88**, 1129 (2000).

[15] D. Nguyen-Manh, D. G. Pettifor, D. J. H. Cockayne, M. Mrovec, S. Znam, and V. Vitek, Bull. Mater. Sci. **26**, 43 (2003).

[16] M. I. Baskes, J. E. Angelo, and C. L. Bisson, Modell. Simul. Mater. Sci. Eng. **2**, 505 (1994).

[17] D. Nguyen-Manh, D. G. Pettifor, and V. Vitek, Phys. Rev. Lett. **85**, 4136 (2000).

[18] N. A. Marks, Phys. Rev. B **63**, 035401 (2000).

[19] A modified dihedral term avoids a well-known discontinuity in the original formulation. In the notation of Ref. 3 our dihedral contribution to the bond order is $b_{ij}^{\mathrm{dh}} = 2T_{ij}(N_i^t, N_j^t, N_{ij}^{\mathrm{conj}}) \sum_{k_1(\neq i,j)} \sum_{k_2(\neq i,j)} \sum_{l_1(\neq i,j)} \sum_{l_2(\neq i,j)} (1-\cos^2(\theta_{ijkl})) f_c(r_{ik_1}) f_c(r_{ik_2}) f_c(r_{il_1}) f_c(r_{il_2})$, similar to Ref. 29. Here $\cos\theta_{ijkl} = \vec{e}_{jik12} \cdot \vec{e}_{ijl12}$ and $\vec{e}_{jik12} = \vec{r}_{ji} \times \vec{r}_{k_1 k_2}$.

[20] D. A. Drabold, P. A. Fedders, and P. Stumm, Phys. Rev. B **49**, 16415 (1994).

[21] D. G. McCulloch, D. R. McKenzie, and C. M. Goringe, Phys. Rev. B **61**, 2349 (2000).

[22] T. Frauenheim, P. Blaudeck, U. Stephan, and G. Jungnickel, Phys. Rev. B **48**, 4823 (1993).

[23] D. S. Franzblau, Phys. Rev. B **44**, 4925 (1991).

[24] A slight improvement of the unscreened BBOP can be achieved by simply increasing the cutoff to $r_1 = 1.95$ Å and $r_2 = 2.25$ Å as in Ref. 14. This does not cure bond breaking.

[25] R. Pérez and P. Gumbsch, Phys. Rev. Lett. **84**, 5347 (2000).

[26] R. Pérez and P. Gumbsch, Acta Mater. **48**, 4517 (2000).

[27] E. Bitzek, P. Koskinen, F. Gähler, M. Moseler, and P. Gumbsch, Phys. Rev. Lett. **97**, 170201 (2006).

[28] Our plane-wave DFT calculations using the CASTEP code (Ref. 30) and employing generalized gradient approximation (Ref. 31), ultrasoft pseudopotentials (Ref. 32), and a plane-wave cutoff of 350 eV were converged to 0.01 eV/Å mean force, 0.001 Å displacement, and $10^{-6}$ eV total energy. Forces for Brenner and DFTB were converged to $10^{-4}$ eV/Å.

[29] J. H. Los, L. M. Ghiringhelli, E. J. Meijer, and A. Fasolino, Phys. Rev. B **72**, 214102 (2005).

[30] CASTEP 4.2 Academic Version, licensed under the UKCP-MSI Agreement, 1999; M. C. Payne, M. P. Teter, D. C. Allan, T. A. Arias, and J. D. Joannopoulos, Rev. Mod. Phys. **64**, 1045 (1992).

[31] J. P. Perdew, J. A. Chevary, S. H. Vosko, K. A. Jackson, M. R. Pederson, D. J. Singh, and C. Fiolhais, Phys. Rev. B **46**, 6671 (1992).

[32] D. Vanderbilt, Phys. Rev. B **41**, 7892 (1990).